integrity Research Journals

Applied Journal of Physical Science
Volume 6(3), pages 73-90, June 2025
Article Number: 57D229653
ISSN: 2756-6684
https://doi.org/10.31248/AJPS2025.116
https://integrityresjournals.org/journal/AJPS

Full Length Research

Assessment of geothermal resource potentials at some parts of Central Benue, Nigeria, using aeromagnetic and radiometric data

Ejike K. Nnaemeka[1]*, Gabriel N. Egwuonwu[1], Orji Obinwa[2], Chiagozie C. Onyekwelu[1] and Nneji G. Ezenwa[1]

[1]Department of Physics and Industrial Physics, Nnamdi Azikwe University Awka, Anambra State, Nigeria.
[2]Department of Physics, Clifford University, Owerrinta, Nigeria.

*Corresponding author. Email: ejikekings24@gmail.com

Received 5th April 2025; Accepted 8th May 2025

ABSTRACT: The study presents the results of the assessment and analysis of geothermal heat flow and radiogenic heat contributions of some parts of the central Benue Trough, Nigeria. The assessment and analysis are for probable geothermal energy exploration on a reconnaissance basis employing aeromagnetic and radiometric datasets. The data was analysed to determine the geothermal energy potential of the area and its possible utilisation for improved access to power. The interpretation of aeromagnetic data comprises subdivision of the total magnetic field reduced to the equator (TMI_RTE) into twenty-five equal (25) overlapping spectral blocks of 55×55 km windows. Hence, spectral analysis via fast Fourier transform (FFT) was executed for each overlapping spectral blocks and depths to the centroid and top boundary of magnetic bodies were obtained from the plots of the log of spectral energies against wave number. The results obtained from depths to the centroid and top boundary (Z_0 & Z_t) were used to compute the Basal depth (Curie point depth). The Curie point depth ranges from 8.18 to 41.45 km with an average value of 16.39 km. Geothermal gradient and heat flow estimated from CPD using an average thermal conductivity of 2.17 $Wm^{-1}{}^{\circ}C^{-1}$ gave values ranging from 13.99 to 70.90°C/km (average of 42.18 °C/km) and 30.36 to 153.85 mWm^{-2} (average of 91.96 mWm^{-2}), respectively. The result for the radiogenic heat generation ranged from 0.9 to 2.90 μWm^{-3}. In summary, the study shows combine high geothermal heat flow and radiogenic heat contributions from both datasets signifying probable geothermal sources, viable for geothermal energy exploration in the southeastern, northeastern, southwestern and top northern parts of the area, such as Ihugh, Katsina-Ala, Wuse, Otupko, Otobi Lafia, Giringwe, and Agyaragu.

Keywords: Airborne radiometric, geothermal energy, heat flow, magnetic, radiogenic heat.

INTRODUCTION

Integration of geophysical methods is usually adopted extensively to determine subsurface crustal structures of the earth that may support exploration of hydrocarbons, solid minerals, heat flow analysis for geothermal exploration, geological problems and other economic materials deposited beneath the earth's surface. The application of airborne geophysical techniques such as gravity, magnetics and radiometrics is based on contrasting physical properties of rocks such as density contrast, magnetic susceptibility and radioactivity (Kearey *et al*., 2002). Thus, recently, these geophysical methods can be adopted in early stages of investigations via delineation of various geological phenomena, structural configuration, geothermal energy potential, hydrocarbon prospecting and mineral exploration. The magnetic method in particular has been shown to be the most cost-effective geophysical method of producing models for geothermal structures (Mohammadzadeh-Moghaddam *et al.,* 2016). Its data as a potent tool can be used to probe the subsurface (Ejiga *et al.,* 2021; Abdullahi and Kumar, 2020).

Since, heat of magmatic rocks are buried in the crust and the some energy, practically comes from the radioactive decay of rocks in the mantle, this has positioned the

magnetic and radiometric as the best methods in early stage of geothermal energy prospecting because of their unique ability to map, curie depth, heat flow, basement structures, hydrothermal areas related to heat flow routes and radiogenic heat production associated with radioactive elements of potassium thorium and uranium. In understanding the thermal system beneath the Earth's surface, good knowledge of thermal conductivity and heat production of geological formations is needed. The main sources of this heat flow emanating from the Earth's interior are derived from the processes of the formation of earth and decay of radioactive isotopes such as potassium, uranium and thorium (Kearey *et al*., 2002; Vacquier, 1998; Benkhelil, 1989).

This created an opportunity for the use of the two airborne geophysical data (aeromagnetic and aero-radiometric) in this study to delineate spots within the area of study with possible geothermal energy resource potential. Since geothermal energy is environmentally friendly, affordable, sustainable and a renewable form of energy, that can be exploited for direct use (heating) and electricity generation. Some geophysical investigations on geothermal energy have been carried out within the Benue trough using aeromagnetic and aero-radiometric datasets (Olorunsola and Aigbogun, 2017; Ayuba and Nur, 2018; Aliyu *et al*., 2018; Abdullahi and Kumar, 2020; Tende *et al*., 2021; Ngene *et al*., 2022) to map/delineate geothermal sources on a reconnaissance basis. Then, within the central Benue trough, scholars such as Aigbedion *et al*. (2022), Egwuonwu *et al*. (2023), and Alfaifi *et al*. (2023) employed spectral depth techniques of aeromagnetic data and got heat flow values ranging from 69.68 to 194.87 mWm^{-2}, 40.23 to 177.03 mWm^{-2}, and 95 to 235 mWm^{-2}, respectively. Also, Akinnubi and Adetona (2018), Salako *et al*. (2020) and Ayatu *et al*. (2023) used combined methods of magnetic and radiometric datasets and obtained heat flow and radiogenic heat values from 76.6 to 153.35 mWm^{-2} &1.47 to 2.21 μWm^{-3}; 50.02 to 85.1 mWm^{-2} and 1.58 to 2.53 μWm^{-3}; 38.96 to 114.17 mWm^{-2} and 1.27 to 2.4 μWm^{-3}, respectively.

The evidence of geothermal energy potential on the surface of the earth can be manifested as hot springs, mud-pools, geysers, steaming grounds, altered grounds and fumaroles (Ochieng, 2013). Some known hot surface springs manifestations located in the Cretaceous central Benue Trough, namely, Keana-Awe Thermal spring, Akiri Warm spring, and Ruwan Zafi, influenced the choice of the current study to investigate the geothermal energy potential of the central Benue Trough.

This study is aimed at assessing the geothermal resource potentials at some parts of the central Benue Trough, for probable geothermal energy exploration, by engaging integrated approaches of combining airborne magnetic and radiometric datasets. Some areas, such as Ihugh, Katsina-Ala, Wuse, Otupko, Otobi Lafia, Giringwe, and Agyaragu within the study area showed favourable geothermal energy potentials.

Location and geology of the study area

The central Benue Trough is part of the general linear NE-SW trending Benue Trough Basin. It has an estimated coverage area of about 165 × 165 km. It is located within north central Nigeria between latitudes 7°00' and 8°30' N and longitudes 8°00' and 9°30′ E (Figure 1). Geology of the Benue Trough has been discussed by many scholars (Reyment, 1965; Cratchley and Jone, 1965; Short and Stauble, 1967; Murat, 1972; Nwachukwu, 1972; Olade, 1975; Whiteman, 1982; Obaje, 2004). They described the Benue Trough as an inland sedimentary basin in Nigeria that forms as a part of the more extensive Central African rift system, and resulted from the rifting of the Central and West African basement uplift during the early Cretaceous (Obaje, 2004).

The study area has six (6) Cretaceous sedimentary formations (lithology units) of Nkporo, Agwu, Lafia–Wukari, Eze-Aku, Asu-River and Bima formations. The six formations consist of shale, mudstone, limestone, sandstone, sandy shale, siltstone, feldspathic sandstone, calcareous sandstone, black shale, shelly limestone and sandstone intercalations. There are also exposures of basement rocks which intruded into the sedimentary beds, as seen in Figure 2. The basement rock lithology is mainly rhyolite, porphyritic granite, biotite granite, quartzite and undifferentiated schists, including phyllites, banded gneiss/biotite, migmatite, porphyroblast gneiss, silicified large quartz veins and sheared rocks.

MATERIALS AND METHODS

Nine (9) half-degree by half-degree aeromagnetic and radiometric data sheets for the following locations: "Doma (230), Lafia (231), Akiri (232), Agana (250), Makurdi (251), Akwana (252), Otupko (270), Gboko (271) and Katsina Ala (271)" were obtained from the Nigeria Geological Survey Agency (NGSA), Abuja. These datasets were acquired between the years of 2005 and 2009 as part of the airborne survey conducted in Nigeria by Fugro Airborne Surveys Canada. A flying height of 0.1 km, a flight line spacing of 0.5 km, and a tie line spacing of 5 km were employed during data acquisition. This digital data was provided in 55×55 km sheets at a scale of 1:100,000. "The Oasis Montaj 8.4, ArcGIS 10.5, MATLAB 15, and Surfer 15" software programs were used for analysing and interpreting these data for the research.

Spectral techniques of aeromagnetic data

The spectral analysis technique has been widely employed in the investigation of geothermal energy sources when using potential field data, like the magnetic data, to determine Curie point depth (basal depth), geothermal gradient and heat flow of any area of interest.

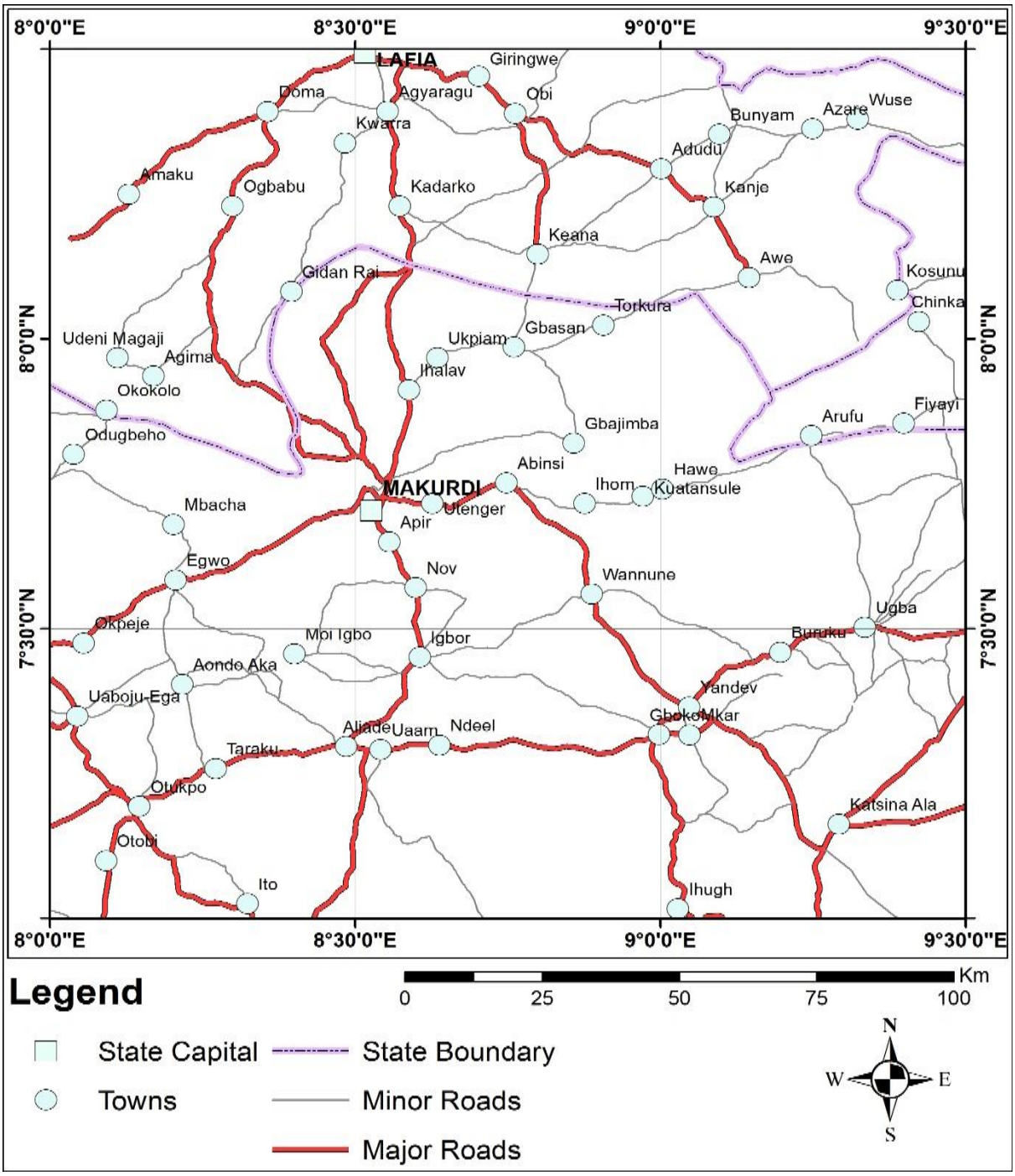

Figure 1. Location map of the study area.

This is because the spectral technique allows estimation of the depth of magnetised blocks of varying thickness, width, depth and magnetisation (Tanaka *et al.* 1999; Spector and Grant, 1970). According to the assertions of Spector and Grant (1970) on the spectral depth technique, the gradient of the log of the power spectrum can be used to calculate the depth to the top of a magnetic square prism (Z_t). Later, using the knowledge from Spector and Grant (1970), Bhattacharyya and Leu (1975, 1977) made the first estimation of the centroid depth of magnetic sources (Z_0). To that end, Okubo *et al.* (1985) developed methods for calculating the depth to the bottom of magnetic bodies (Z_b) by integrating and extending the ideas of Spector and Grant (1970) and Bhattacharyya and Leu (1977). The Fast Fourier Transform (FFT), which computes the Discrete Fourier Transform (DFT), is the mathematical tool

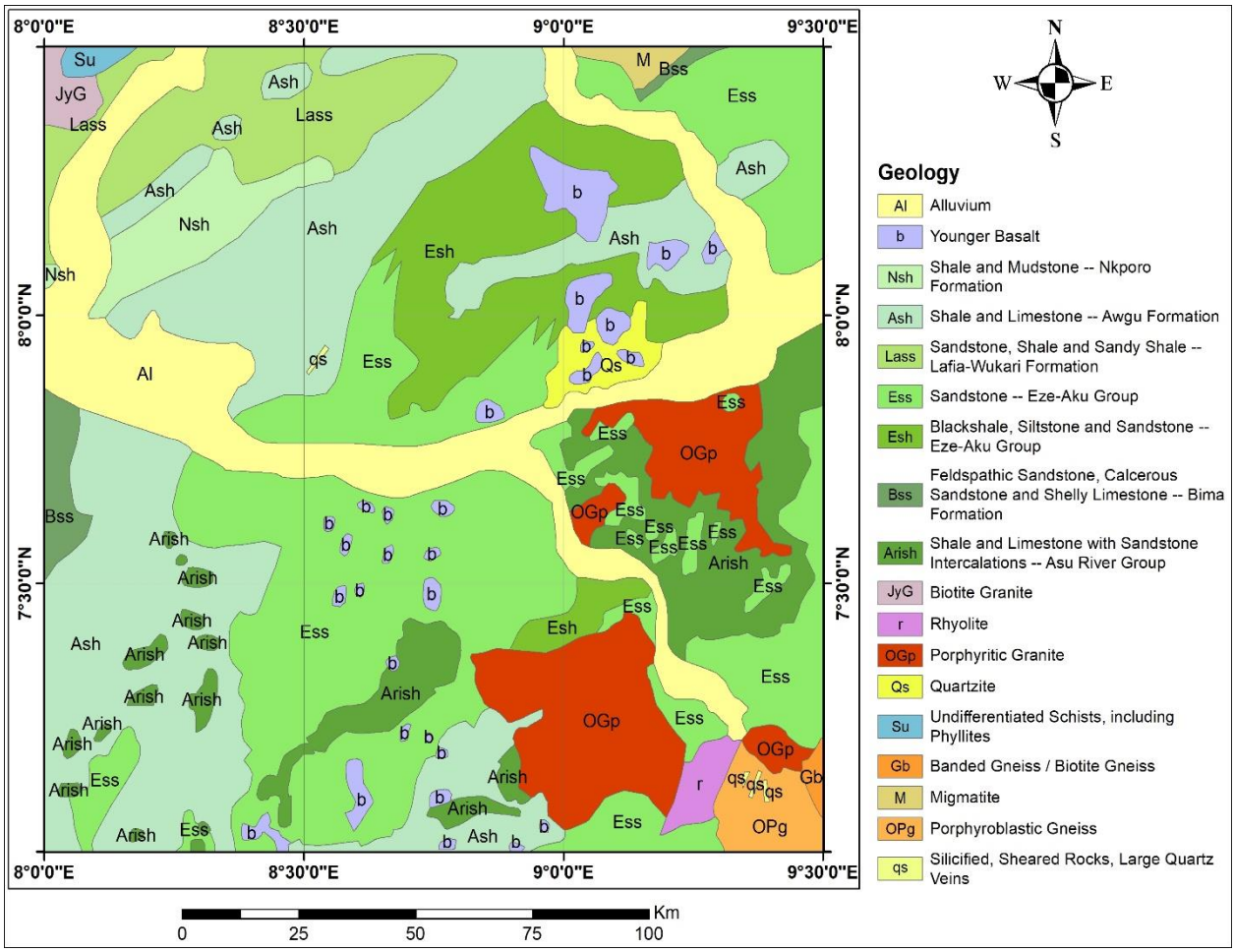

Figure 2. Geology map of the study area.

(algorithm) used for the spectral depth analysis of regularly spaced data, such as airborne potential field data. This algorithm, when applied to airborne geophysical data, converts the spatial or real space data to a frequency domain. (Telford *et al.,* 1990). The advantage of the Spectral technique, according to Telford *et al*. (1990), is its ability to filter almost all the noise from the data, with no information disappearing during data processing by overlapping the data operations, which are easier and better in the transform domain.

The work of Okubo *et al*. (1985) stated that the basal depth, also known as the depth to the bottom of a magnetic source (Z_b), can be obtained in two phases. Firstly, evaluating the deeper magnetic source from the slope of the longest wavelength part of the spectrum divided by the wave number, equation (1) below (Okubo *et al*., 1985).

$$\ln\left[\frac{\sqrt{P_{(s)}}}{|s|}\right] = \ln A - 2\pi|s|Z_o \quad (1)$$

Where $P_{(s)}$ is the radially mean power spectrum of the anomaly, *A* is assumed to be a constant |s| is the wave number and Z_0 is depth to the centroid.

Secondly, is to estimate the depth to the top of magnetic body Z_t from the slope of the higher wavenumber part of the spectrum.

$$\ln\left[\sqrt{P_{(S)}}\right] = \ln B - 2\pi|s|Z_t \quad (2)$$

P is the power spectral density; B is total amount of constant quantity independent of |s| and Z_t is the depth to top boundary (basement depth).

The depth to the bottom of magnetized body (Curie point depth), which is the depth that describes the inferred curie point transition of magnetite (Nur *et al*.,1999) is therefore obtained as follows (Okubo *et al*., 1985):

$$Z_b = 2Z_0 - Z_t \quad (3)$$

Where: Z_b is the depth to the bottom of the magnetised

body (Curie point depth), Z_0 is the depth to the centroid, and Z_t is the depth to the top boundary (basement depth).

According to Tanaka *et al*. (1999, 2005) and Stampolidis *et al*. (2005), the depth to the bottom of the magnetic body is related to the Curie temperature (580°C). The geothermal gradient, as suggested by Tanaka *et al.* (1999, 2005) and Stampolidis *et al*. (2005), can be calculated using equation (4) below, and this expresses that equation (5) stated below was used to calculate the geothermal gradient of the study area.

$$\theta = \left(\frac{dT}{dZ}\right) Z_b \quad (4)$$

The equation 4, the geothermal gradient $\left(\frac{dT}{dZ}\right)$ can be expressed as;

$$\frac{dT}{dZ} = \frac{\theta}{Z_b} \quad (5)$$

Assuming that the direction of a temperature variation is vertical in a one-dimensional case and the thermal gradient$\left(\frac{dT}{dZ}\right)$ is constant. The geothermal heat flow can be calculated using equation (6)

$$q_z = k\frac{dT}{dZ} \quad (6)$$

Where q_z is heat flow, $\boldsymbol{\theta}$=580°C (Curie temperature value), Z_b is Curie point depth, and thermal conductivity k = 2.17 $Wm^{-1}\ ^0C^{-1}$. The choice of the thermal conductivity was based on the average thermal conductivity for sedimentary 1.8 $Wm^{-1}\ ^0C^{-1}$ and igneous rocks 2.54 $Wm^{-1}\ ^0C^{-1,}$ being the most predominant rock found in the area of study as detailed in the geology map of the area (Figure 2).

Application of the spectral techniques to the airborne magnetic data

The TMI_RTE map of the study area was subjected to spectral analysis by dividing the map into twenty-five equal overlapping spectral blocks, as follows: block A-Y of a spectral probe measuring 55 km by 55 km. According to Nwankwo and Shehu (2015), taking smaller window sizes in spectral analysis of potential field data, might produce an error in interpretations for the depth to the top boundary (basement depth), so the 25 blocks obtained ensured 50% overlapping, and the block size (window) was chosen to avoid fundamental error. Each of the 25 blocks was subjected to the Log of Power Spectrum filtering method of the Oasis Montaj software, using the Fast Fourier Transform (FFT) algorithm, which assisted in converting the airborne magnetic data from real space to the frequency domain. The (SPC) energy files of the 25 blocks were input into a spectral program plot (SPP) created with MATLAB. This action generated the plots of the logarithm of spectral energy ln (E) against the wave number (cycle/km). This program was created specifically to get the gradients for the depths to the centroid and the top of the magnetic body.

Analysis of radiogenic heat production

As asserted by Kearey *et al*. (2002), the radiometric method obtains an exceptional radioactive result in the mapping of various kinds of geological formations. This technique allows the calculation of the heat produced during radioactive decay of Uranium, Potassium and Thorium within the rocks. This is because the rocks producing the radiogenic heat are often targets for geothermal exploration and production. The natural byproducts of the decay series of the radioactive elements uranium, thorium, and potassium are found in sedimentary rocks in varying concentrations, and the heat produced varies significantly with lithology because of variations in the concentration of the three radioelements eU, eTh, and %K (Čermák and Rybach 1982; Haack 1982). The scholarly publication of Holmberg *et al*. (2012) opined that, since the majority of the continental heat flow comes from the decay series of radioactive isotopes in the crust. That by implication, locating areas with high heat flow can be the same as locating areas of high radioactive heat generation. The radiogenic heat production Q (μWm^{-3}) by radioactivity in rocks that have concentrations C_K (%), C_{Th} (ppm) and C_u (ppm) for potassium, thorium and uranium, respectively, was expressed mathematically by (Rybach, 1976) as given in equation (7). This equation will be employed in computing the radiogenic heat production of the area. Hence, compare its result with that of the aeromagnetic and ascertain its effectiveness in mapping the geothermal system of the area based on a reconnaissance aspect.

$$Q\ (\mu Wm^{-3}) = \rho\ (0.0348C_K + 0.0257C_{Th} + 0.0953C_U) \quad (7)$$

Q is the radiogenic heat production, while ρ is the average density of the rocks in the area, C_K (%), C_{Th} (ppm) and C_u (ppm) are average concentrations of the radioactive isotopes.

RESULTS AND DISCUSSION

The total magnetic intensity (Figure 3) and reduced to the equator (RTE) maps (Figure 4) of the study area displayed high and low magnetic anomaly distributions between -58.49 and 99.80 nT and -53.92 and 96.97 nT, respectively. The high magnetic anomalies (pink colours) distribution across the study area is attributed to shallow basements/ structures or areas of intrusions observed majorly at NE-SW trend, while the low magnetic anomalies (blue colours)

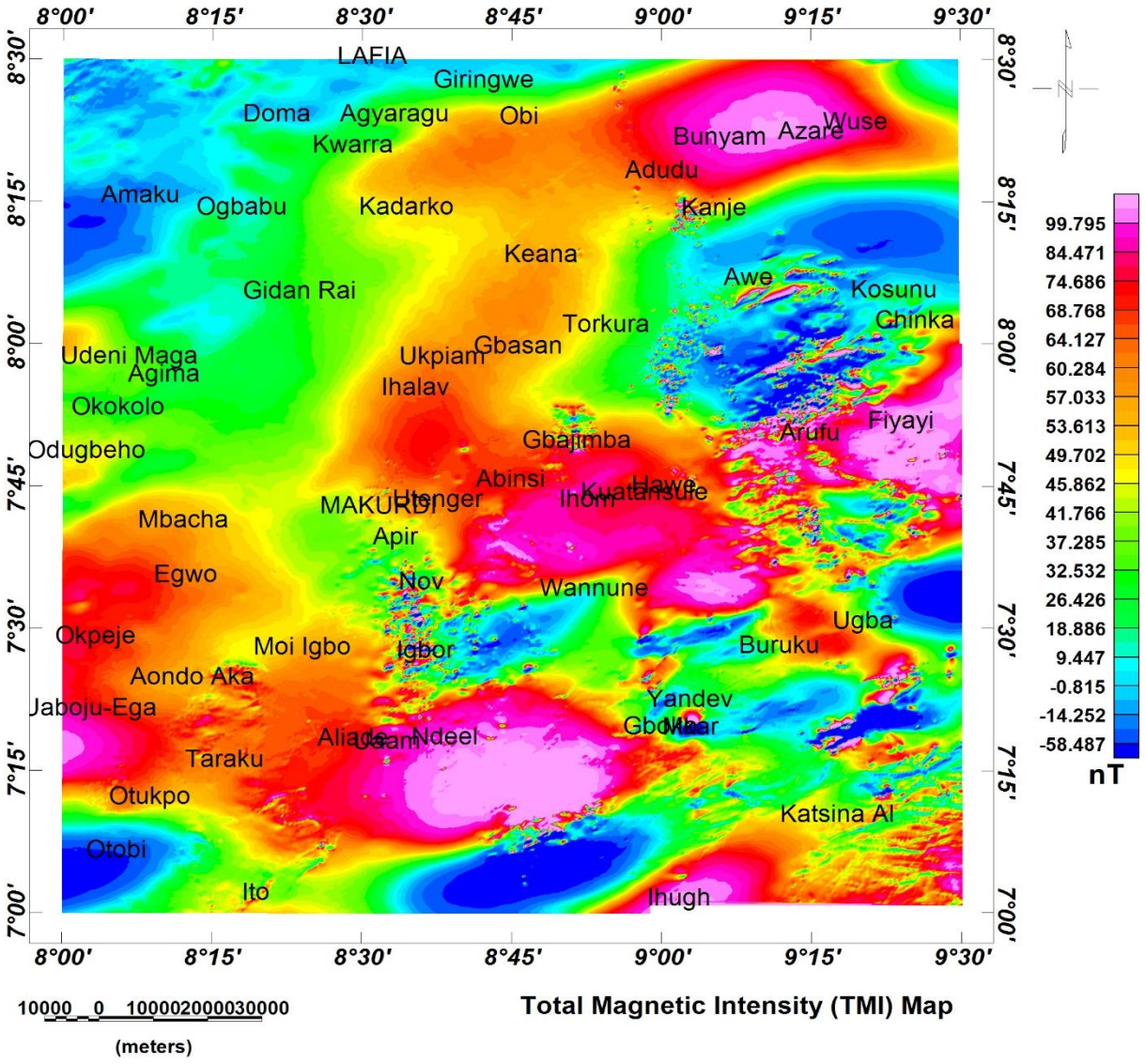

Figure 3. Total magnetic intensity map of the area.

depict areas with deep structures/magnetic sources or areas with thick sedimentary cover.

Both maps showed similar trends of anomaly strikes, but the RTE shows a clearer display of magnetic signatures than the TMI map. The RTE map was used for the spectral analysis to calculate Curie point depth, geothermal gradient and heat flow of the area, which can be used to locate areas with geothermal energy potential.

Intrepretations of basal depth, geothermal gradient and heat flow maps

Using centroid depth (Z_0) and depth to the top boundary (Z_t), Curie point depth (basal depth) was computed employing equation (3), which was developed by (Okubo *et al*., 1985; Tanaka *et al*., 1999). The results for (Z_0) and (Z_t), respectively, were derived by plotting logarithm of spectral energy ln (E) against the wave number (cycle/km) (Figure 5a and b). The results of the centroid depth, depth to the top, computed CPD values, geothermal gradient, and heat flow from spectral cells of 55×55 km are shown in Table 1.

Curie point depth map

CPD values range from 8.18 to 41.45 km, with a mean value of 16.39 km. The contour maps shown (Figure 6a and b) reflected deeper CPD at southwestern, southeastern, and northeastern areas with the deepest value around Gboko, Yandev and Mkar areas, indicated with black square dotted lines (Figure 6a). This result obtained agrees with the work of Akinnubi and Adetona

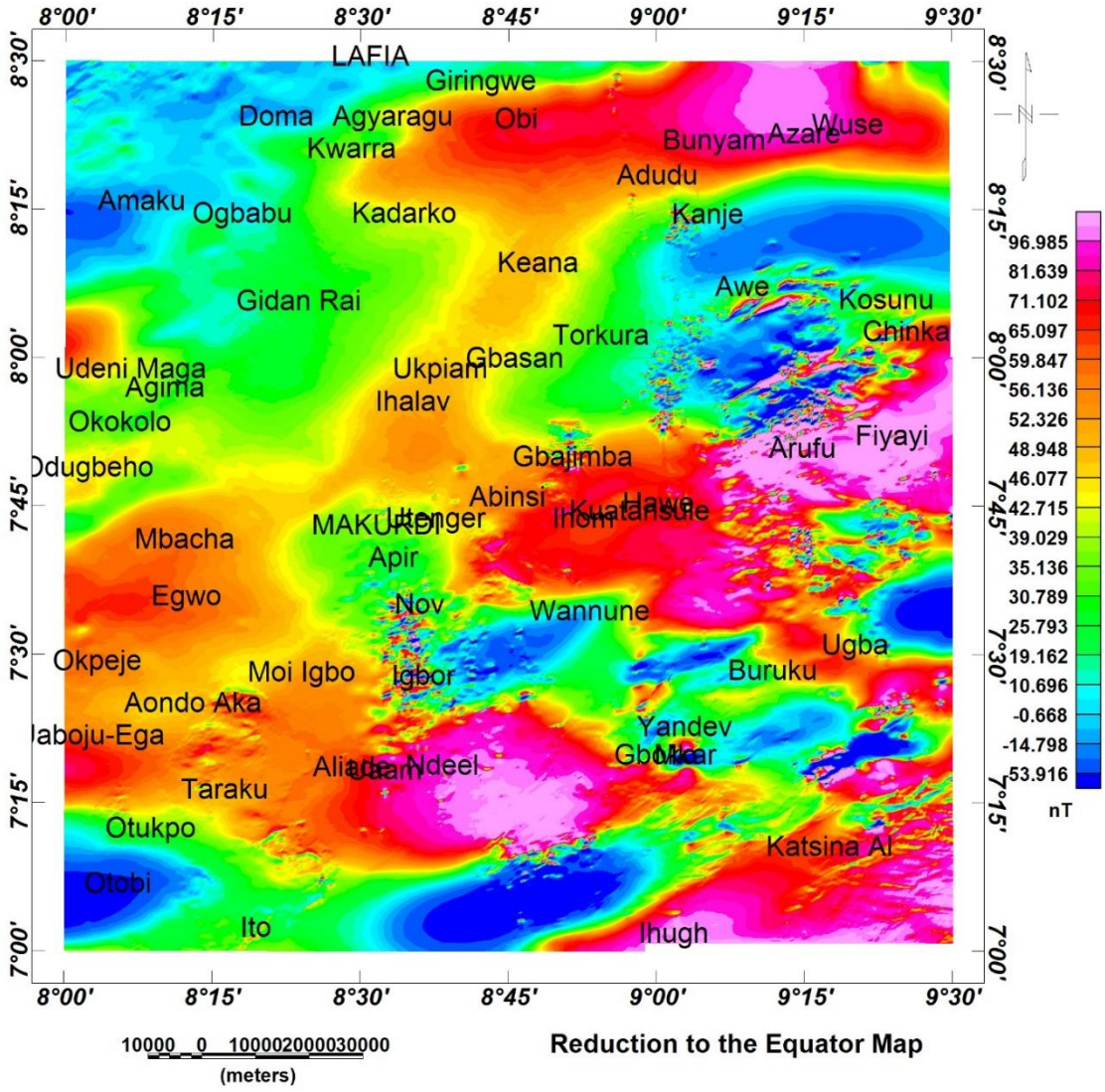

Figure 4. Reduction to the equator map of the area.

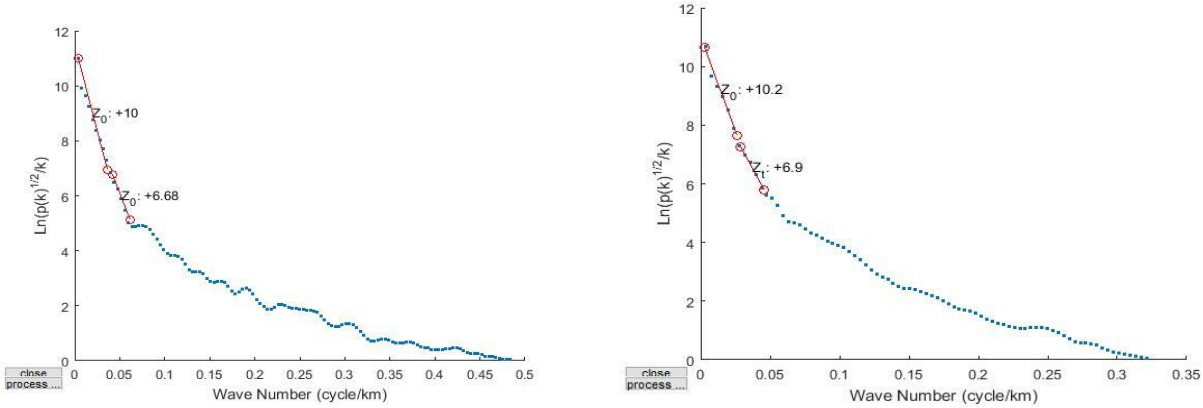

(a) (b)

Figure 5 (a and b). Samples of the 25 (A-Y) spectral blocks of 55 × 55 km.

Table 1. Results of the centroid depth, depth to the top, calculated values Curie point depth, geothermal gradient and heat flow from spectral cells of 55× 55 km.

Blocks	Longitude (°)	Latitude (°)	Centroid depth (km)	Depth to the top (km)	(Curie point) (km)	Geothermal gradient (^{0}C/km)	Heat flow (HF) (mWm^{-2})
A	8.25	8.25	10.0	6.68	13.32	43.54	94.48
B	8.50	8.25	10.2	6.90	13.50	42.96	93.22
C	8.25	8.25	13.3	7.70	18.90	30.69	66.60
D	9.00	8.25	12.2	3.59	20.81	27.87	60.48
E	9.25	8.25	8.55	3.90	13.20	43.94	95.35
F	8.25	8.00	8.03	4.56	11.50	50.43	109.43
G	8.50	8.00	6.07	3.20	8.94	64.88	140.79
H	8.75	8.00	6.45	1.86	11.04	52.54	114.01
I	9.00	8.00	7.06	2.75	11.37	51.01	110.69
J	9.25	8.00	8.32	2.37	14.27	40.64	88.18
K	8.25	7.75	7.64	3.99	11.29	51.37	111.47
L	8.50	7.75	6.18	3.68	8.68	66.82	150.0
M	8.75	7.75	6.29	2.39	10.19	56.82	123.30
N	9.00	7.75	7.98	2.51	13.45	43.12	93.57
O	9.25	7.75	7.58	3.76	11.40	50.88	110.41
P	8.25	7.50	6.10	3.84	8.18	70.90	153.85
Q	8.50	7.50	15.4	3.62	27.18	21.34	46.31
R	8.75	7.50	14.7	1.68	27.72	20.92	45.40
S	9.00	7.50	21.5	1.55	41.45	13.99	30.36
T	9.25	7.50	6.28	2.07	10.49	55.29	119.98
U	8.25	7.25	15.9	2.92	28.88	20.08	43.57
V	8.50	7.25	9.97	3.71	16.23	35.73	77.53
W	8.75	7.25	15.7	3.74	27.66	20.97	45.50
X	9.00	7.25	7.19	1.73	12.65	45.85	99.49
Y	9.25	7.25	10.1	2.07	18.13	31.99	69.42

(2018) who also obtained their deepest CPD value around the Gboko area. The observed CPD distribution may be a result of porphyritic granite that intruded the sedimentary terrain. The shallowest CPD is seen around the northwestern, central and northeastern areas of the study area. Curie point depth (CPD) is dependent on geological conditions as established by Tanaka *et al*. (1999) Bhattacharyya and Leu 1975; Ross *et al*., 2006 such that shallow CPD less than 10 km is considered as volcanic and geothermal spots, while values between 10 and 20 km are associated with island ridges and arches, plateaus, and trenches, respectively.

Geothermal gradient and heat flow maps

The geothermal gradient of the area of study was calculated using a Curie temperature of 580°C and respective CPD values of each block. Estimated values of geothermal gradient range from 13.99 to 70.90 ˚C/km with a mean value of 42.18°C/km. The contour map (Figure 7), revealed high geothermal gradients at the southwestern, northeastern, southeastern, middle and upper northern portions of the study area. The geothermal heat flow of the area was computed using an average thermal conductivity of k = 2.17 Wm^{-1} ^{0}C^{-1}. The results of the geothermal heat flow ranged from 30.36 to 153.85 mWm^{-2} with a mean of 93.16 mWm^{-2}. This closely agrees with the results of Akinnubi and Adetona (2018), Aigbedion *et al*. (2022), Egwuonwu *et al*. (2023), and Ayatu *et al*. (2023. The contour map (Figure 8) revealed geothermal heat flow values of 60 to 100 mWm^{-2} at the southwestern (Otupko, Otobi, Ito and Aondo-Aka), northeastern (Arufu, Bunyan, Azare, Wuse, Kosonu, Chinka, Adudu, Kanje and Fiyayi), southeastern (Ugba, Ihugh and Kastina- Ala), central (Wannune, Igbor, Nov, Moi- Igbo, Hawe, Ihom and Kuatansule) and northern parts (Obi, Agyaragy, Lafia and Giringwe) of the study area. These heat flow values (60 to 100 mWm^{-2}) are considered to be good for geothermal energy prospecting as established by Jessop *et al*. (1976). Geothermal heat flow value >100 mWm^{-2} is considered an anomalous geothermal heat flow condition (Jessop *et al*., 1976). This anomalous geothermal heat flows of (>100 mWm^{-2}) are observed at the northwestern, southwestern and some central parts of the study area, such as Giden Rai, Udeni-Magaji, Agima, Okokolo, Odugbeho, Mbacha,

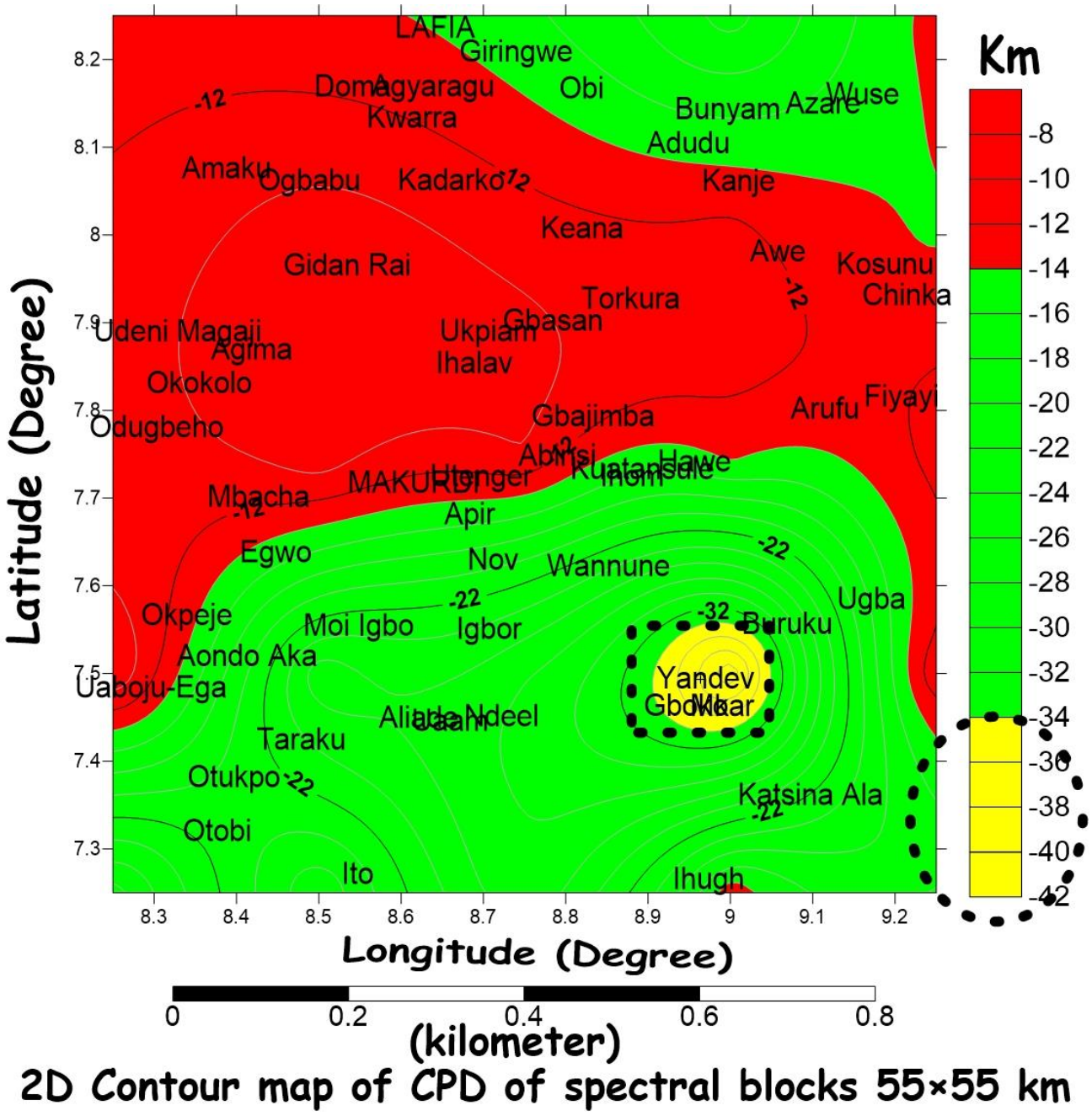

Figure 6a. Contour map of Curie point depth of the study area (Black dotted lines = area with deepest CPD).

Abinsi, Gbajimba, Torkura, Egwo, Makurdi, Utenger, Apir, Okpeje, Uaboju-Ega, Ihalav, Ukpiam, Gbajimba, Gbasan, Kakarko, Amaku, Ogbabu, Kwara and Doma. Also, low geothermal heat flow is seen at the southern part of the study area in places such as Aliade, Ndeel, Uaam, Gboko, Mkar, Yandev, Buruku and Taraku. A correlation of linear relationship was noticed between the geothermal gradient and heat flow maps, depicting areas of high geothermal gradient corresponding to areas of high heat flow and vice versa.

Interpretations of equivalent Uranium (eU), Potassium (%) and Thorium (eTh) Maps

Potassium (%K) concentration map

The potassium concentration map (Figure 9a) revealed three levels of K-concentration - high, low and very low concentrations. The high concentrations ranging from 1 to 2.3% are recorded at the north eastern, central, southeastern, and northwestern parts of the study area.

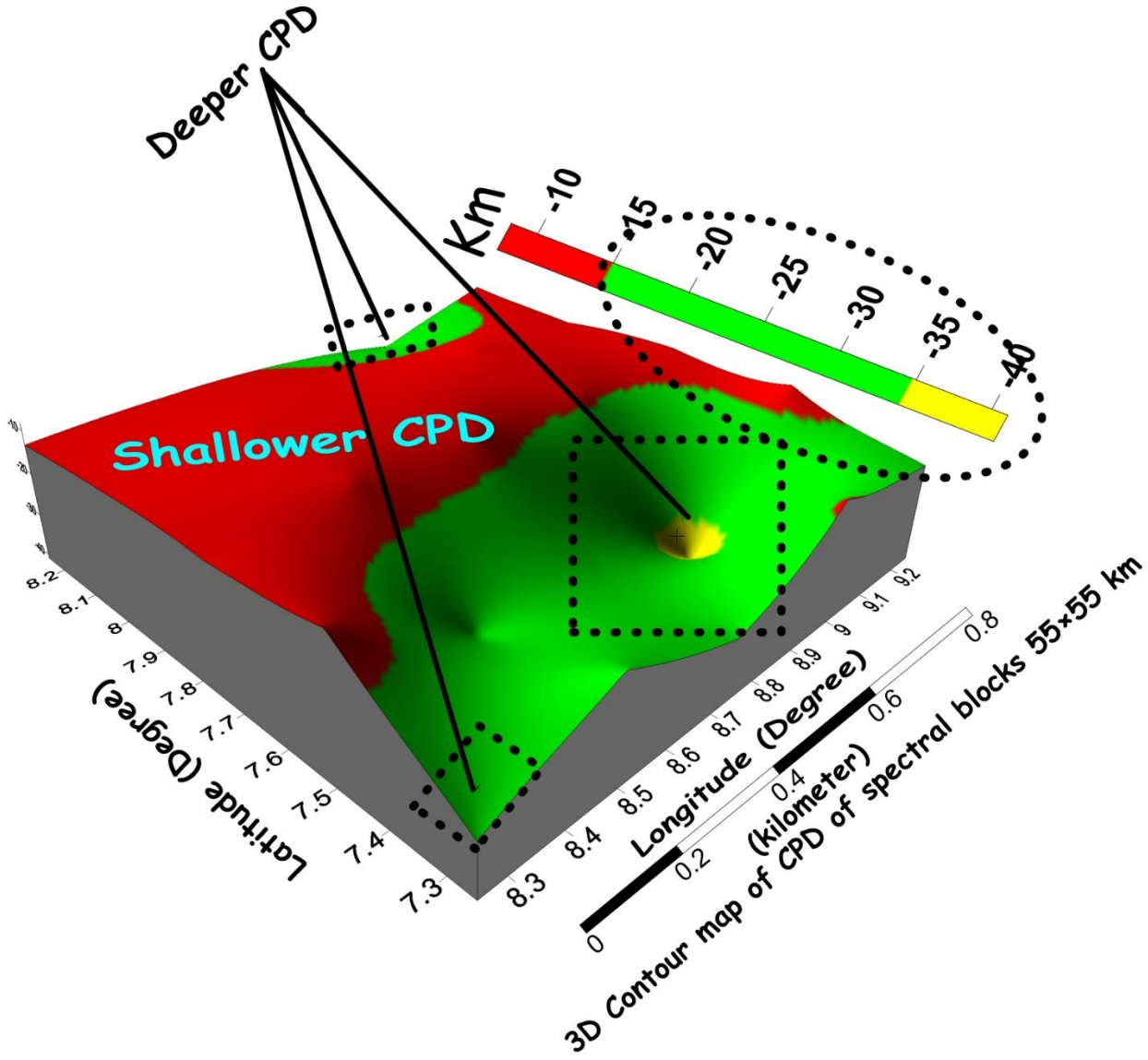

Figure 6b. 3D contour map of Curie point depth of the study area.

This high K-concentration may be attributed to the dominance of igneous intrusive bodies of porphyritic granite, porphyroblastic gneiss, younger basalt, biotite granite, undifferentiated schists, including phyllites and alluvium deposits, as observed in the geology map (Figure 2) of the area. The low K-concentrations with values from 0.2 to 0.9 % observed at the SW, NW and southern portions of the area could be dominance of Agwu formation (shale and limestone), Lafia-Wukari formation (sandstone and shale) and fragments of Bima and Asu-River formations (sandstone, limestone and shales) (Figure 2). The very low K-concentrations ranging from 0.1 to 0.2% recorded more at NNW parts of the study, such as Doma, Gidan Rai, Amaku, Lafia, Agyaragu and Ogbabu, may be attributed to Lafia-Wukari formation (sandstone and shale) and Npkoro formation (shale and mudstone). Hence, it is suggested from the study that high concentrations of potassium are related to deposits of alluvium and igneous intrusive rocks and low concentrations are associated with sedimentary rocks of shale, limestone, sandstone and mudstone.

Thorium (eTh) concentration map

The equivalent thorium (eTh) concentration map (Figure 9b) shows that the distribution of the eTh concentrations is variable, widely spread and distributed all over the various lithological units of the study area. High, low and very low concentrations of eTh are observed all over the study area.

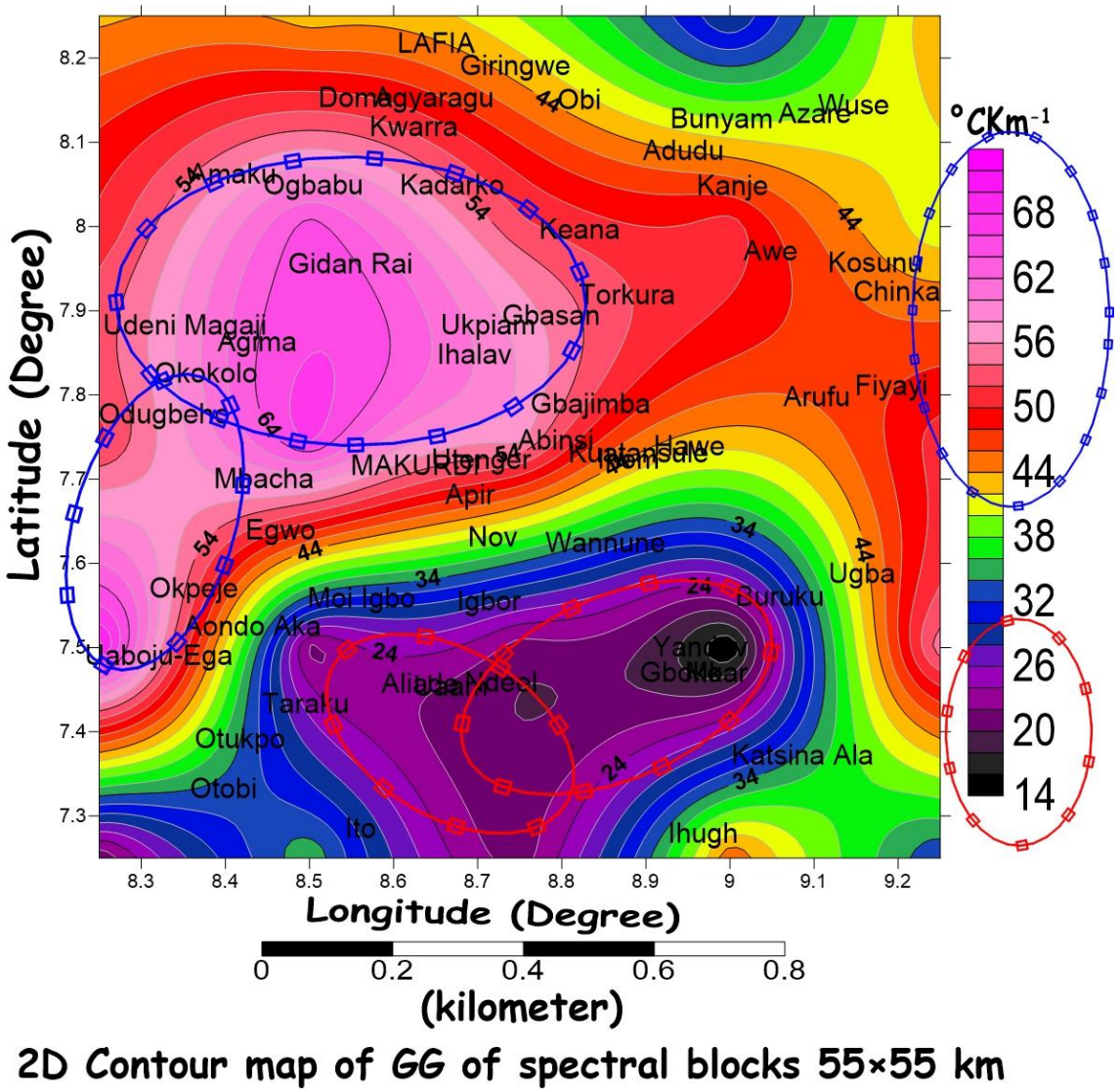

Figure 7. contour map of geothermal gradient of the study area (Blue rings = areas with highest geothermal gradients values; Red rings = areas with lowest geothermal gradients values).

This effect may be associated with the abundance and immobile nature of thorium in the Earth's crust. The high concentration of thorium is recorded at the southeastern, northwestern, northeastern and southwestern areas. The very low concentration that is more pronounced at the northwestern parts and north-central directions of the area may be due to the occurrence of Nkporo Formation (shale and mudstone), alluvium deposits and Lafia-Wukari formation (sandstone and shale) (Figure 2).

Uranium (eU) concentration map

The Uranium concentration map (Figure 9c) shows a high and low concentration distribution all over the various lithological units of the study area. These similar features were also observed on the eTh concentration map (Figure 9b) of the area. The high uranium concentrations are reflected in the southeastern, northwestern, northeastern and southwestern areas. The very low concentrations (1.1 to 1.7 ppm) that are predominant at the northwestern parts and north-central directions of the study area may be associated with Nkporo formation (shale and mudstone), alluvium deposits and Lafia-Wukari formation (sandstone and shale).

Interpretation of the radiogenic heat production of the study area

The radiogenic heat production (RHP) was estimated from the mean concentrations of %K, eU and eTh in the study

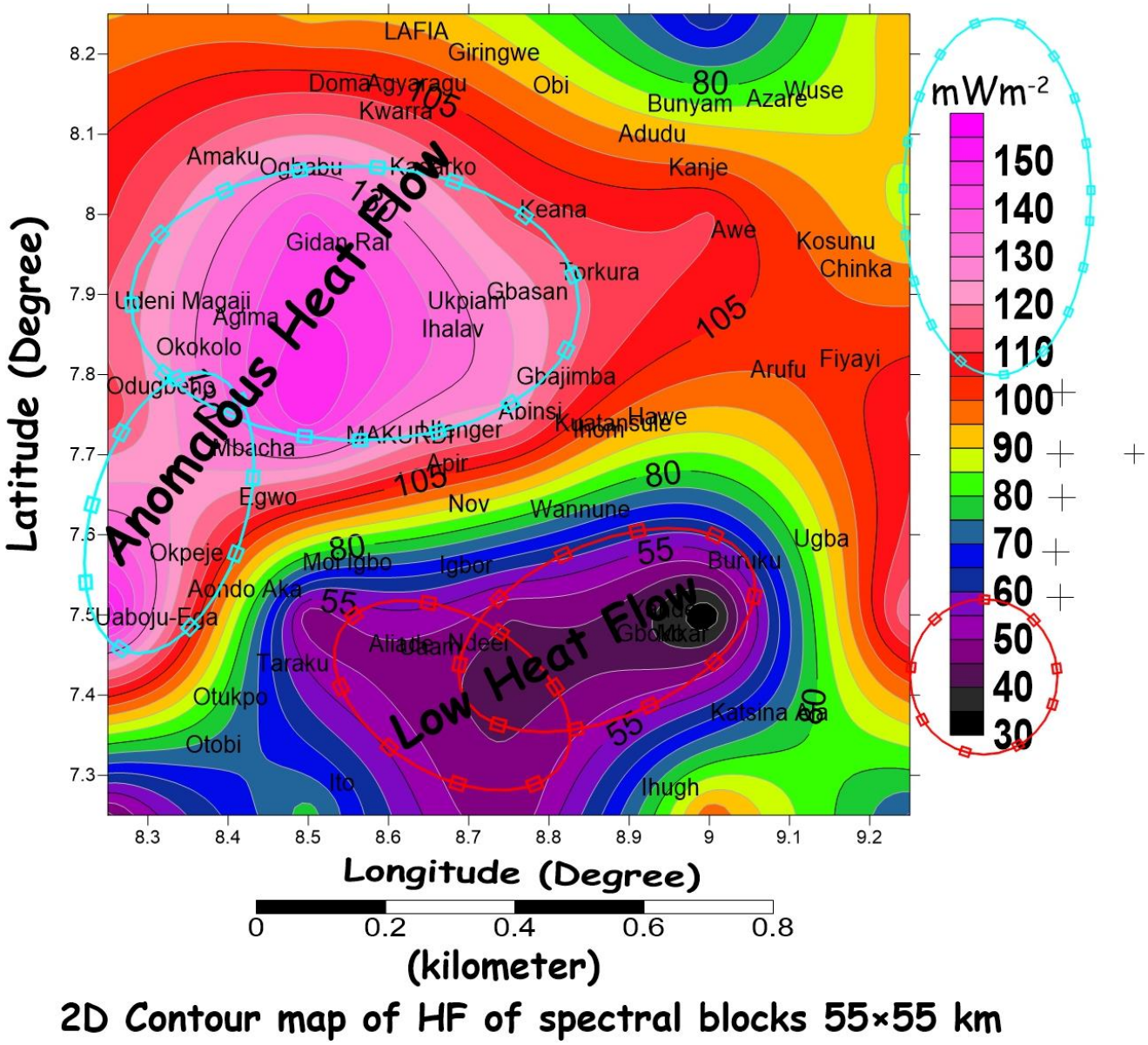

Figure 8. Contour map of heat flow of the study area [Sky blue rings = highest geothermal heat flow areas (anomalous heat flows); Red rings = lowest geothermal heat flow areas.

area, adopting equation 7. The three radioelement concentration (%K, eU and eTh) maps of the study area were tied vertically alongside the geology map (Figure 2). Forty-five (45) profiles, five profiles each, were drawn on nine lithology units: Nkporo formation, Agwu formation, Lafia–Wukari formation, Eze-Aku group (Esh), Eze-Aku group (Ess), Asu-River group, Bima formation, alluvium and porphyritic granite to obtain the average concentration values of the three radioactive elements C_K (%), C_U (ppm), C_{Th} (ppm) and mean total count of each of the lithological units found in the study area as presented in Table 2. In computing the radiogenic heat production of the area, the average density of the rock units alongside the mean concentration of each element were calculated via equation 7 (Rybach, 1976). The radiogenic heat production ranges between 0.9 to 2.9 μWm^{-3}. The RHP contour map (Figure 10) showed high mean radiogenic heat signatures >2.25 $\mu Wm^{-3,}$ indicating probable geothermal sources. Rybach (1986) suggest that the minimum required radiogenic heat flow signifying geothermal source for younger sedimentary and granitic rocks is 2.25 μWm^{-3} and any value in excess of this 2.25 μWm^{-3} indicates geothermal sources that are only crustal in nature without contributions of heat from the mantle as recorded at the southwestern (Okpeje, Uaboja –Ega, Otupko, Otobi, and parts of Aondo-Aka), northeastern (Wuse), southeastern (Ihugh and Kastina- Ala), central (Keana) and top northern parts (Agyaragy, Lafia and

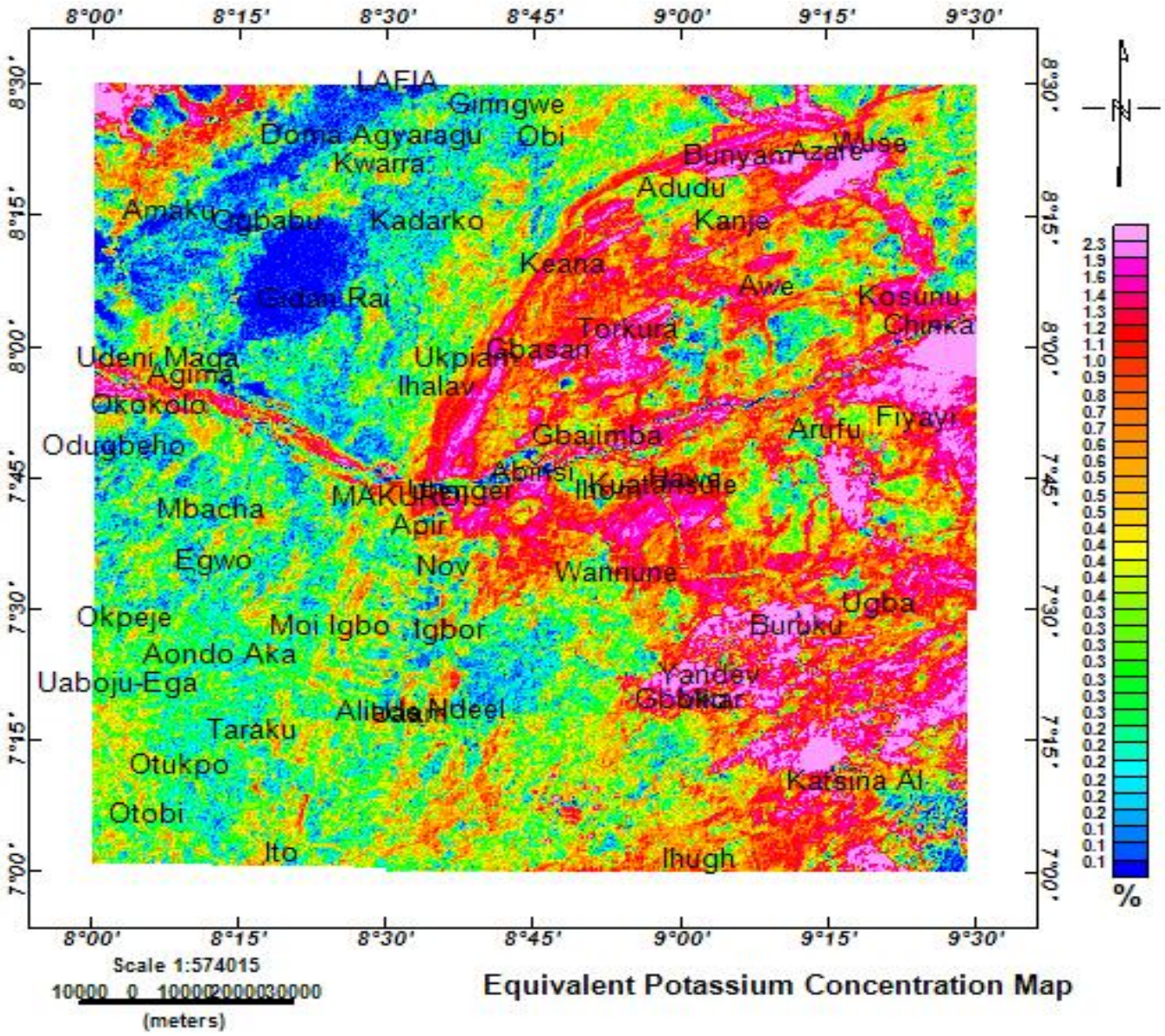

Figure 9a. Potassium concentration map of the study area.

Giringwe). The lowest RHP (0.9 to 1.3 μWm^{-3}) observed at the southwestern parts corresponding to Gidan Rai, Ogbabu and Amaku may be attributed to the combined low effect of the three radioelements (Figure 9a, b and c). The result of our study agrees with the results of Akinnubi and Adetona (2018), Salako *et al*. (2022), and Ayatu *et al*. (2023), who have worked in parts of the Central Benue Trough using airborne radiometric data.

Integration of the results of airborne magnetic and radiometric datasets for geothermal exploration

According to Rybach (1986), radiogenic heat productions in sedimentary rocks depend on important situations that affect their heat flow and thermal history. It can be inferred from the results of the interpretations of the airborne geophysical datasets that the area showed viability for geothermal energy potentials. A very good correlation is observed from the close examination of the geothermal heat flow (Figure 8) and radiogenic heat production (Figure 10) maps of the area. The areas with an acceptable threshold of 60 to 100 mWm^{-2} for probable geothermal sources closely correspond with areas of high radiogenic heat flow, which ranges from 2.3 to 2.9 μWm^{-}3, signifying potential for geothermal energy (Rybach, 1986) within the study area. The integration and correlation between the two heat flow maps positioned the southeastern, northeastern and southwestern and northern parts of the study area, Otupko, Otobi, Wuse, Ihugh and Kastina-Ala,

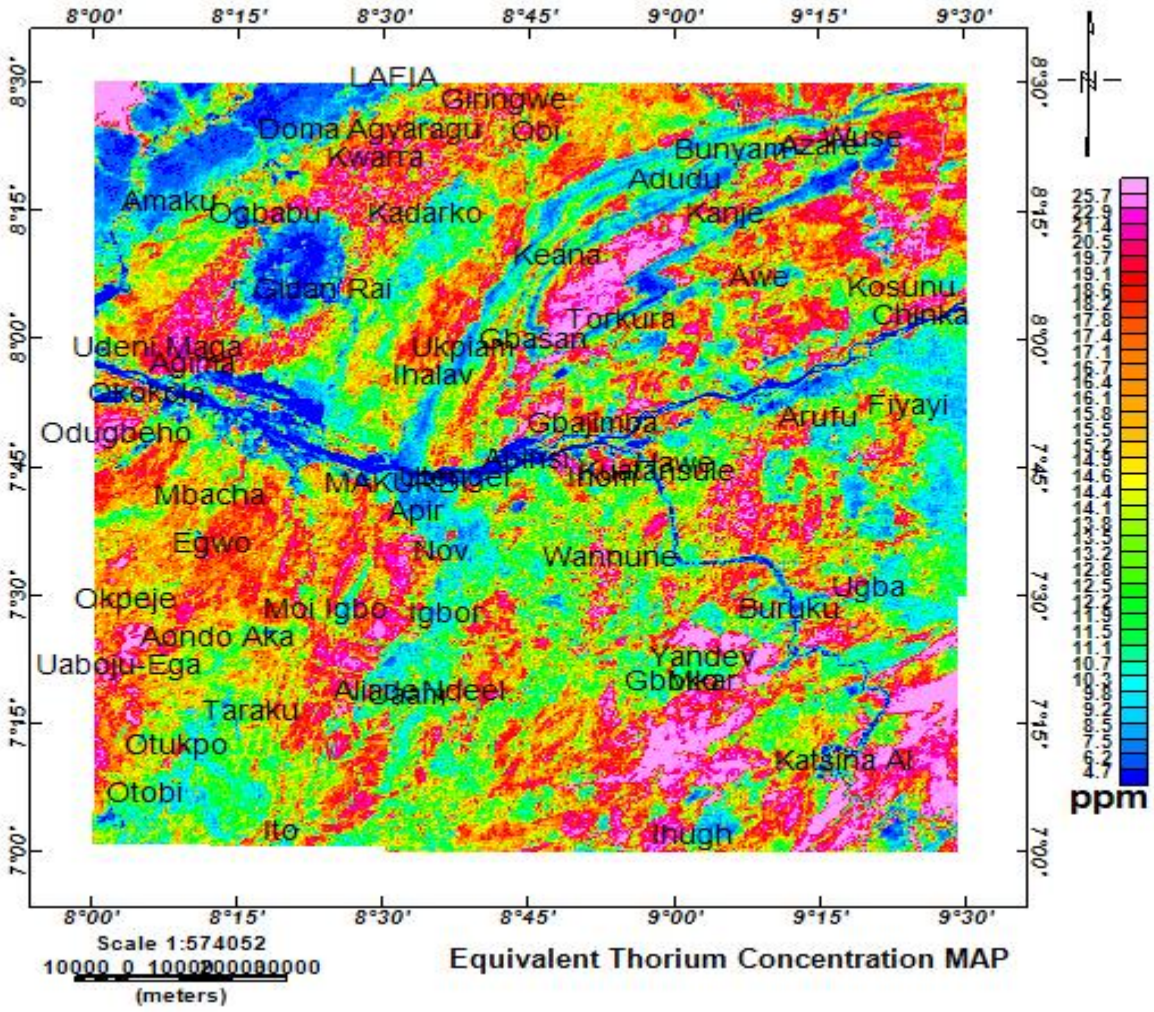

Figure 9b. Equivalent Thorium concentration map of the study area.

Table 2. Results of the mean concentrations of K (%), eU (ppm), eTh (ppm), TC and RHP (μWm^{-3}).

Lithology	Sample No	Long. (°)	Lat. (°)	Mean C_k (%)	Mean C_{Th}(ppm)	Mean C_u (ppm)	Mean total count	RHP (μWm^{-3})
Lafia-Wakari Formation	LWF1	8.64	8.34	0.20	10.30	3.30	13.80	2.50
Lafia-Wakari Formation	LWF2	8.83	8.45	0.50	17.40	5.10	23.00	2.40
Lafia-Wakari Formation	LWF3	8.39	8.36	0.30	12.30	4.00	16.60	2.10
Lafia-Wakari Formation	LWF4	8.27	8.33	0.30	18.00	5.20	23.50	1.80
Lafia-Wakari Formation	LWF5	8.45	8.34	0.20	11.4	3.70	15.30	2.40
Nkporo Formation	NF1	8.32	8.17	0.20	12.30	5.70	18.20	0.90
Nkporo Formation	NF2	8.23	8.10	0.30	17.00	5.50	22.80	2.80
Nkporo Formation	NF3	8.13	8.06	0.20	13.70	4.10	18.00	2.70
Nkporo Formation	NF4	8.20	8.09	0.10	12.90	4.10	17.10	2.30
Nkporo Formation	NF5	8.24	8.15	0.20	18.80	6.40	25.40	1.90
Agwu Formatiom	AF1	8.63	8.16	0.30	13.00	3.90	17.20	2.00
Agwu Formatiom	AF2	8.07	7.38	0.30	14.80	4.40	19.50	2.40
Agwu Formatiom	AF3	8.22	7.48	0.30	13.80	3.60	17.70	2.40
Agwu Formatiom	AF4	8.81	7.12	0.30	15.70	4.80	20.80	2.30
Agwu Formatiom	AF5	9.21	8.17	0.30	16.90	4.90	22.10	2.40

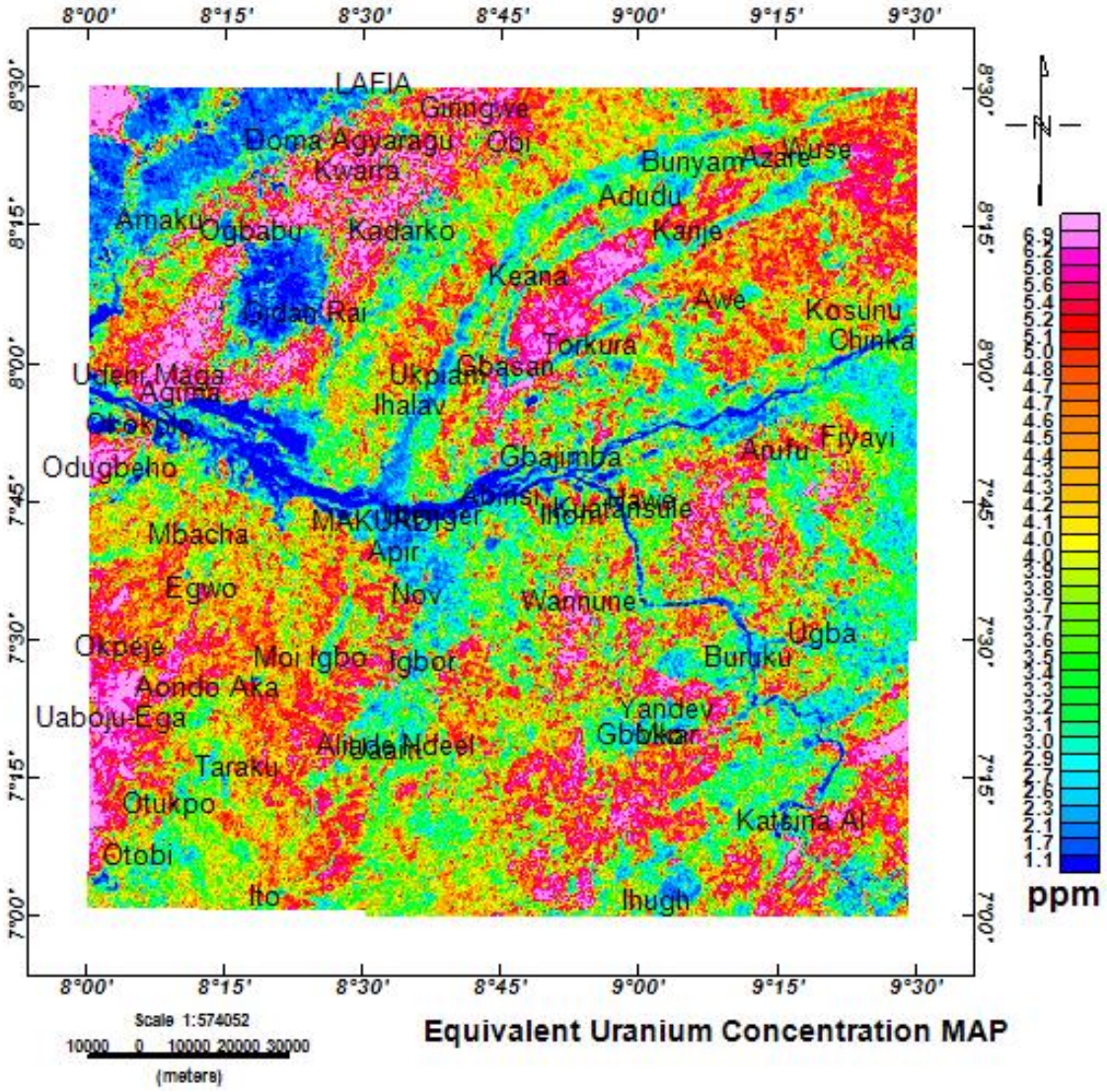

Figure 9c. Equivalent Uranium concentration map of the study area.

Table 2. Contd.

Eze-Aku Group (Esh)	EA1	8.84	8.15	1.00	13.50	3.90	18.40	2.50
Eze-Aku Group (Esh)	EA2	8.84	8.22	0.70	16.30	4.70	21.70	1.80
Eze-Aku Group (Esh)	EA3	8.80	7.91	1.20	14.80	3.90	19.90	2.10
Eze-Aku Group (Esh)	EA4	9.08	8.29	0.70	11.80	3.90	16.40	1.90
Eze-Aku Group (Esh)	EA5	9.18	7.99	0.80	16.00	4.60	21.40	2.10
Eze-Aku Group (Ess)	EA6	9.47	8.28	0.30	14.20	4.10	18.60	2.30
Eze-Aku Group (Ess)	EA7	8.62	7.90	0.80	13.50	3.70	18.00	1.80
Eze-Aku Group (Ess)	EA8	8.62	7.60	0.50	14.80	4.00	19.30	2.10
Eze-Aku Group (Ess)	EA9	9.40	7.32	0.80	13.80	3.20	17.80	2.90
Eze-Aku Group (Ess)	EA10	8.66	7.47	0.30	18.30	4.90	23.50	1.90
Bima Formation	BF1	8.02	7.72	0.20	20.40	6.50	27.10	2.30
Bima Formation	BF2	8.03	7.62	0.50	16.20	4.60	11.30	2.40
Bima Formation	BF3	8.03	7.55	0.20	15.40	4.50	20.10	2.60
Bima Formation	BF4	8.02	7.64	0.60	14.10	3.80	18.50	2.30
Bima Formation	BF5	9.25	8.45	0.80	11.60	3.40	15.80	2.30

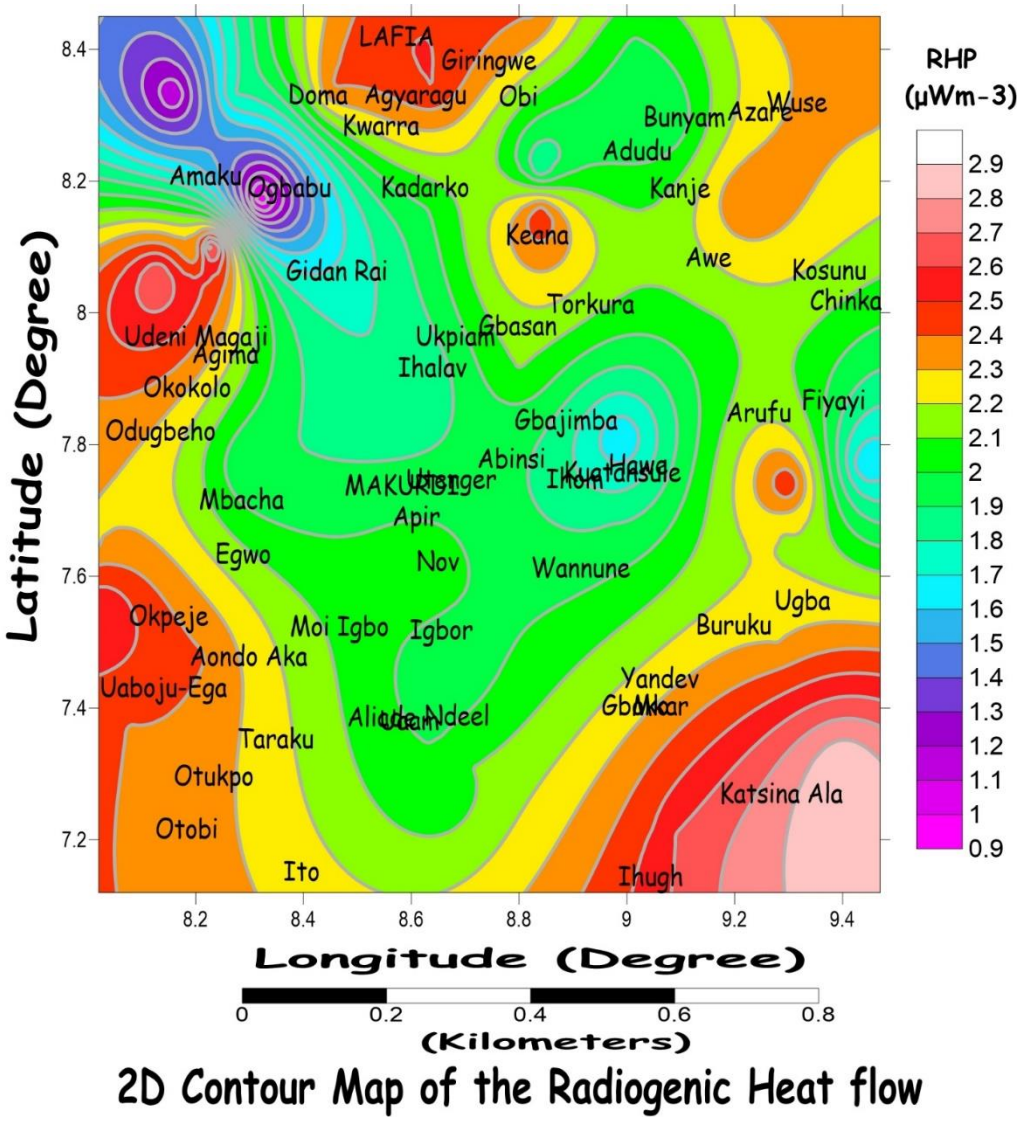

Figure 10. Radiogenic heat flow map of the study area.

Table 2. Contd.

Asu- River Group	AG1	8.67	7.28	0.40	15.20	4.20	19.80	2.00
Asu- River Group	AG2	9.44	7.77	0.60	18.00	4.10	22.70	1.60
Asu- River Group	AG3	9.28	7.50	1.30	11.30	3.50	16.10	2.30
Asu- River Group	AG4	9.28	7.50	0.80	14.60	4.00	19.40	1.70
Asu- River Group	AG5	8.71	7.31	1.20	15.40	3.90	20.50	2.10
Basement Rock (QG_P)	PG1	9.09	7.21	0.40	20.80	4.70	25.90	2.60
Basement Rock (QG_P)	PG2	9.05	7.22	0.70	14.90	4.20	19.80	2.50
Basement Rock (QG_P)	PG3	9.30	7.74	1.00	19.90	4.40	25.30	2.50
Basement Rock (QG_P)	PG4	9.29	7.67	2.00	11.50	3.50	17.00	2.20
Basement Rock (QG_P)	PG5	9.01	7.12	1.30	14.50	4.40	20.20	2.50
Alluvium Deposit	AL1	8.29	7.77	0.50	7.30	2.10	9.90	1.90
Alluvium Deposit	AL2	8.16	8.33	0.70	13.00	3.60	17.30	1.10
Alluvium Deposit	AL3	8.97	7.68	0.90	14.40	4.00	19.30	1.90
Alluvium Deposit	AL4	8.99	7.81	0.40	11.60	2.90	14.90	1.60
Alluvium Deposit	AL5	9.01	8.42	1.10	14.30	3.80	19.20	2.00

Agyaragy, Lafia and Giringwe as the most viable areas for geothermal energy exploration. This is because the areas mentioned indicated both high geothermal heat flow and high radiogenic heat flow. Curie point depth is dependent on geological conditions (Tanaka *et al*.,1999; Bhattacharyya and Leu, 1975; Ross *et al*., 2006) as radiogenic heat is dependent on the variations in concentrations of K (%), eU (ppm), eTh (ppm) in the rock types (Čermák and Rybach, 1982; Haack, 1982). The areas with low heat flow and radioactive heat contributions are observed from central to southern parts of Taraku, Ito, Aliade, Ndeel, Uaam, Yandev, Mkar, Gboko, Buruku and Igbor.

Correlation of the viable geothermal energy exploration areas with the geology map

The viable areas indicated by both methods are the Southeastern, Northeastern, Southwestern and top northern parts of the investigated area is attributed to dominance of Agwu formation (shale and limestone), Lafia- Wukari formation (sandstone and shale), Bima formations (sandstone and limestone), igneous intrusive bodies of porphyritic granite, porphyroblastic gneiss, younger basalt, quartzite, rhyolite and undifferentiated schists, including phyllites, banded gneiss/biotite, migmatite, silicified large quartz veins, sheared rocks and Eze-Aku sandstone which produced the highest radiogenic heat value (Table 2). Hence, the study reveals that, place of combined high geothermal and radiogenic heat flows may be attributed to igneous intrusive rocks and sedimentary rocks of shale, limestone, and sandstone. This closely agrees with the research of Kuforrijimi and Olorunsola and Aigbogun (2017), who investigated radiogenic heat production in the lower part of the Benue Trough, Nigeria (Anambra basin) and observed that shale is the rock with the highest radiogenic production.

Conclusion

Analysis and interpretations of the two aero-geophysical datasets employed for the study successfully helped in mapping the geothermal energy signatures of the Central Benue Trough, Nigeria. Results showed a good correlation between heat flow and radiogenic heat production, such that areas of high heat flow correspond with areas of high radiogenic heat production. It can be understood from the two interpreted results of the two airborne geophysical datasets (magnetic and radiometric) used for the study that have detected probable geothermal energy exploration targets in this region on a reconnaissance basis. In light of this, it is recommended that the exploration target areas identified at the southeastern, northeastern, southwestern and top northern areas of study, such as Otupko, Otobi, Wuse, Ihugh, Kastina-Ala, Agyaragy, Lafia and Giringwe, be further explored for geothermal energy development. . This is because, if it is further explored and harnessed, due to its advantage of constant availability in the earth's subsurface, it will help reduce the electricity challenges ravaging the country due to the prevalent challenging factors such as population, industrialisation and excess demand for electricity. It's also a clean form of energy that is environmentally friendly, that may not constitute gas emissions or deplete the ozone layer, as in line with the international standard and policies on energy.

CONFLICT OF INTEREST

The authors declare that they have no conflict of interest.

REFERENCES

Abdullahi, M., & Kumar, R. (2020). Curie depth estimated from high-resolution aeromagnetic data of parts of lower and middle Benue trough (Nigeria). *Acta Geodaetica et Geophysica*, *55*(4), 627-643.

Aigbedion, I., Aikhuele, D. O., Salufu, S. O., & Aigbedion, E. O. (2022). Innovative geothermal energy assessment of Akiri and environs for clean energy generation in Nigeria. *Asian Journal of Geoscience*, *30*, 100-115.

Akinnubi, T. D., & Adetona, A. A. (2018). Investigation of the geothermal potential within Benue State, central Nigeria, from radiometric and high-resolution aeromagnetic data. *Nigeria Journal of Physics 27*(2), 2018-2019.

Alfaifi, H. J., Ekwok, S. E., Ulem, C. A., Eldosouky, A. M., Qaysi, S., Abdelrahman, K., Andráš, P., & Akpan, A. E. (2023). Exploratory assessment of geothermal resources in some parts of the Middle Benue Trough of Nigeria using airborne potential field data. *Journal of King Saud University-Science*, *35*(2), 102521.

Aliyu, A., Salako, K. A., Adewumi, T., & Mohammed, A. (2018). Interpretation of high-resolution aeromagnetic data to estimate the Curie point depth isotherm of parts of the middle Benue trough, northeast, Nigeria. *Physical Science International Journal*. 17(3), 1-9.

Ayatu, U. O., Kumbur E. B., Onwuemesi A. G., Anakwuba, E. K., & Chinwuko A. I. (2023). Evaluation of geothermal energy potential of parts of the Middle Benue trough Nigeria: aeromagnetic and aeroradiometric approach. *Iranian Journal of Geophysics*, *16*(4), 37-52.

Ayuba, R. A., & Nur, A. (2018). Determination of curie depth isotherm and geothermal studies over parts of Nasarawa and environs, North Central Nigeria. *International Journal of Energy and Environmental Science*, *3*(4), 69-81.

Benkhelil, J. (1989). The origin and evolution of the Cretaceous Benue Trough (Nigeria). *Journal of African Earth Sciences (and the Middle East)*, *8*(2-4), 251-282.

Bhattacharyya, B. K., & Leu, L. K. (1975). Analysis of magnetic anomalies over Yellowstone National Park: mapping of Curie point isothermal surface for geothermal reconnaissance. *Journal of Geophysical Research*, *80*(32), 4461-4465.

Bhattacharyya, B. K., & Leu, L. K. (1977). Spectral analysis of gravity and magnetic anomalies due to rectangular prismatic bodies. *Geophysics*, *42*(1), 41-50.

Čermák, V., & Rybach, L. (1982). Thermal conductivity and

specific heat of minerals and rocks. In: G Angenheister (ed.), Landolt-Börnstein: numerical data and functional relationships in science and technology, new series, Group V *(Geophysics and Space Research),* vol Ia, (Physical Properties of Rocks) pp. 305-343. Springer, Berlin Heidelberg.

Cratchley, C. R., & Jones, G. P. (1965). An interpretation of the geology and gravity anomalies of the Benue valley, Nigeria. *Overseas Geological Surveys Geophysical Paper.* 1, 1-26.

Egwuonwu, G. N., Nnaemeka, E. K., & Orji, O. (2023). Investigating the geothermal energy potentials within the Central Benue Trough Nigeria: Insight from Airborne Potential Field Data. *International Journal of Innovative Science and Research Technology*, *8*(3), 2456-2165.

Ejiga, E. G., Ismail, N. E. H., & Yusoff, I. (2021). Implementing digital edge enhancers on improved high-resolution aeromagnetic signals for structural-depth analysis around the middle benue Trough, Nigeria. *Minerals*, *11*(11), 1247.

Haack, U. (1982). Radioactivity of rocks. In: Hellwege, K. (ed.). Landolt Bornstein numerical data and functional relationships in science and technology. New Series, Group V. Geophysics and Space Research, vol. 1, Physical properties of rocks, sup volume b (pp. 433–481). Springer-Verlag: New York.

Holmberg, H., Naess, E. & Evensen, J. E. (2012). Thermal modeling in the Oslo Rift, Norway. In: *Proceedings of the 37th Workshop on Geothermal Reservoir Engineering, Stanford University*.

Jessop, A. M., Hobart, M. A., & Sclater, J. G. (1976). The world heat flow data collection—1975, Geothermal Series. *Earth Physics Branch, Energetic Mines and Resources, Ottawa, 50*, 55-77.

Kearey, P., Brooks, M., & Hill, I. (2002). *An introduction to geophysical exploration*. Blackwell Science Ltd., London.

Mohammadzadeh-Moghaddam, M., Mirzaei, S., Nouraliee, J., & Porkhial, S. (2016). Integrated magnetic and gravity surveys for geothermal exploration in Central Iran. *Arabian Journal of Geosciences*, *9*, 506.

Murat, R. C. (1972). Stratigraphy and paleogeography of the cretaceous and lower tertiary in Southern Nigeria. In: Dessauvagie T. J. F. & Whiteman, A. J. (eds.). *African Geology*. University of Ibadan Press, Africa. Pp. 251-266.

Ngene, T., Mukhopadhyay, M., & Ampana, S. (2022). Reconnaissance investigation of geothermal resources in parts of the Middle Benue Trough, Nigeria using remote sensing and geophysical methods. *Energy Geoscience, 3*, 360-371.

Nur, A., Ofeogbu, C. O., & Onuoha, K. M. (1999). Estimation of the depth to the Curie point Isotherm in the Upper Benue Trough, Nigeria, *Journal of Mining and Geology*, 35(1), 53-60.

Nwachukwu, S. O. (1972). The tectonic evolution of the Southern portion of the Benue Trough. *Nigeria Geological Magazine, 109*, 411-419.

Nwankwo, L. I., & Shehu, A. T. (2015). Evaluation of Curie-point depths, geothermal gradients and near-surface heat flow from high-resolution aeromagnetic (HRAM) data of the entire Sokoto Basin, Nigeria. *Journal of Volcanology and Geothermal Research*, *305*, 45-55.

Obaje, N. G. (2004). Geology and mineral resources of Nigeria. *Springer Verlag Berlin Heidelberg*, p. 219.

Ochieng, L. (2013). Overview of geothermal surface exploration methods, presented at short course VIII on exploration for geothermal resources, organised by *UNU-GTP, GDC and Ken-Gen, at lake Naivasha, Kenya*, October 31-November 22, 2013.

Okubo, Y., Graf, R. J., Hansent, R. O., Ogawa, K., & Tsu, H. (1985). Curie point depths of the island of Kyushu and surrounding areas Japan. *Geophysics, 53*, 481-494.

Olade, M. A. (1975). Evolution of Nigeria Benue Trough (Aulacogen). *A Tectonic Model, Geomagazine*, *12*, 575-583.

Olorunsola, K., & Aigbogun, C. (2017). Correlation and mapping of geothermal and radioactive heat production from the Anambra Basin, Nigeria. *African Journal of Environmental Science and Technology*, *11*(10), 517-531.

Reyment, R. A. (1965). *Aspects of Geology of Nigeria*. University of Ibadan Press, Ibadan, Nigeria, p. 133.

Ross, H. E., Blakely, R. J., & Zoback., M. D. (2006). Testing the use of aeromagnetic data for the determination of Curie depth in California. *Geophysics, 71*(5), 51–59.

Rybach, L. (1976). Radioactive heat production in rocks and its relation to other Petrophysical parameters. *Pure and Applied Geophysics*, *114*, 309-318.

Rybach, L. (1986). Amount and significance of radioactive heat sources in sediments. In: Thermal Modeling in Sedimentary Basins*: 1st IFP Exploration Research Conference, Carcans, France*. 44 (311). Editions Technip

Salako, K. A., Adetona, A. A., Rafiu, A. A., Alahassan, U. D., Aliyu, A., & Adewumi T. (2020). Assessment of Geothermal potential of parts of the Middle Benue Trough North East Nigeria. *Journal of Earth and Space Physics*, *45*(4), 27-42.

Short, K. C., & Stauble, A. J. (1967). Outline of geology of Niger Delta. AAPG Bull. 51, 761-779.

Spector, A. & Grant, F. S. (1970). Statistical models for interpretation of aeromagnetic data. *Geophysics, 35*, 293-302.

Stampolidis, A., Kane, I., Tsokas, G. N., & Tsourlos, P. (2005). Curie point depths of Albania inferred from ground total field magnetic data. *Surveys in Geophysics*, *26*, 461-480.

Tanaka, A., & Ishikawa, Y. (2005). Crustal thermal regime inferred from magnetic anomaly data and its relationship to seismogenic layer thickness: The Japanese islands case study. *Physics of the Earth and Planetary Interiors*, *152*(4), 257-266.

Tanaka, A., Okubo, Y., & Matsubayashi, O. (1999). Curie point depth based on spectrum analysis of magnetic anomaly data in East and Southeast Asia. *Tectonophysics, 306*, 461-470.

Telford, W. M., Geldart, L. P., & sheriff, R. E. (1990). Applied geophysics. *Cambridge University Press, Second Edition.*

Tende, A. W., Aminu, M. D., & Gajere, J. N. (2021). A spatial analysis for geothermal energy exploration using bivariate predictive modelling. *Scientific Reports*, *11*(1), 19755.

Vacquier, V. (1998). A theory of the origin of the Earth's internal heat. *Tectonophysics, 291*(1-4), 1-7.

Whiteman, A., (1982). Nigeria: Its Petroleum Geology, Resources and Potential*. Graham and Trotham, London.*